Nearfield Noise Identification with a Passive Array in the Underwater Anechoic Basin at KRISO

Sea-Moon Kim, Youngcheol Choi, and Yong-Kon Lim
Korea Research Institute of Ships and Ocean Engineering (KRISO) / KORDI
P. O. Box 23 Yuseong-gu, Daejeon 305-600 Korea
smkim@kriso.re.kr, ycchoi@kriso.re.kr, and yklim@kriso.re.kr

***Abstract*-Unmanned underwater vehicles (UUVs) are used for various underwater missions. During the UUVs' missions sound waves play an important role because acoustic communication and positioning systems are used for the control of the UUVs. However, they do not only have numerous mechanical components but also use hydraulic and electrical systems, which make loud noise and degrade the performance of acoustic equipment. Therefore, we have to examine the noise characteristics before using the acoustic equipment. The investigation method may include localization of the noise sources by using a line array of hydrophones. In order to apply the conventional beamforming algorithm, experiments should be performed in the anechoic environments because it is derived based on the assumption of no reflection. Although KRISO/KORDI has an underwater anechoic basin, it has a free surface that reflects sound waves. Because the acoustic impedance of water is several thousand times bigger than that of air, it is reasonable to assume that it is pressure-released condition. In this paper a source localization method in such a kind of environment is studied. The effects of phase errors are analyzed for plane and spherical wave models. Simulation results say that the estimated position error is negligible if the aperture size is 2.5 times bigger than the wavelength.**

I. INTRODUCTION

In order to perform various underwater acoustic experiments, KRISO/KORDI has constructed a small underwater anechoic basin in 2002 (Fig. 1). It has a rectangular shape and its dimensions are 914cm long, 282cm wide, and 500cm deep. It has cone-type anechoic lining at the four walls and bottom. The sound absorbing materials are made of rubber granules and its shape is designed to absorb acoustic waves which frequencies are higher than about 3kHz [1]. Its main applications are underwater acoustic communications, source localizations, and tests of acoustic equipment being developed. Among them nearfield noise identification is an important application for localizing acoustic sources made by various underwater equipment.

Many kinds of array processing techniques are applied to localize and characterize sound sources, such as beamforming method [2] and matched filed processing (MFP) [3]. Although the MFP has an important role for localizing farfield sources the conventional beamforming method is more efficient for nearfiled souces. However, this method assumes that there is no reflection and multi-path gives the error in the results. Because the anechoic tank does not have anechoic lining at the free surface, sound reflection still happens. This fact leads us to take special care in the use of the conventional beamforming algorithm. Choi and Kim proved that using modified scan vectors gives good results in localization in reverberant fields [4]. They also introduced a special source model which includes infinite number of randomly incident waves [4]. However, the anechoic tank has only one reflection at the free surface. Because the acoustic impedance of water is several thousand times bigger than that of air, it is reasonable to assume that the surface has pressure release condition. In this paper a source localization method in such a kind of environment is studied. In the following section the conventional beamforming method is briefly described. Section III analyzes the effect of phase detection error. Simulation results in free surface evironment are discussed in section IV and Section V concludes this paper.

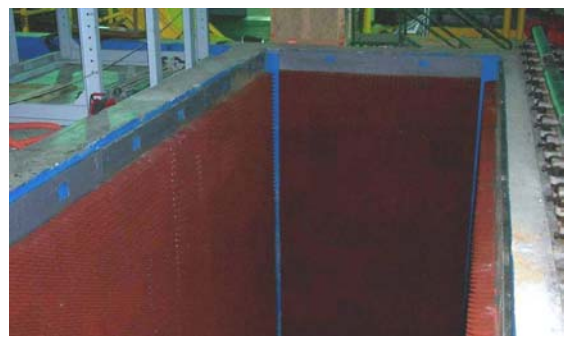

Fig. 1 Photograph of the anechoic tank at KRISO/KORDI before the construction of the test room over the tank (dimensions: 914cm x 282cm x 500cm)

II. CONVENTIONAL BEAMFORMING METHOD

In the conventional beamforming method the source wave model must be defined. According to source locations, plane wave model and spherical wave model are generally used.

A. Plane Wave Model

When a source is far from the array, the propagation pattern at the array can be assumed to be plane (Fig. 2). In this case phase delays between two adjacent hydrophones are same, if the sensors are equally spaced. If there is not any disturbance the pressure at the n-th hydrophone is

$$p_n = Ae^{-jk(n-1)d\sin\theta_0}. \tag{1}$$

The exponential term in Eq. (1) represents phase delay in the frequency domain, which corresponds to time delay in the time domain. The beamforming power is defined as

$$\Pi(\theta) = WRW^H , \tag{2a}$$

where

$$R = E\left[P^H P\right] \tag{2b}$$

$$P = [p_1 \; p_2 \cdots p_N] \tag{2c}$$

$$W = [w_1 \; w_2 \cdots w_N] \tag{2d}$$

$$w_n(\theta) = \frac{1}{\sqrt{N}} e^{-jk(n-1)d\sin\theta} . \tag{2e}$$

The beamforming power is a function of assumed angle θ and has the maximum value at the real incident angle θ_0. Fig. 3 shows an simulation result.

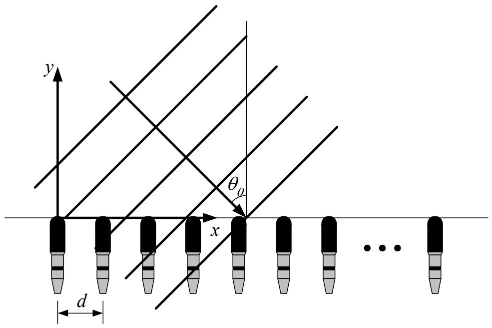

Fig. 2 Plane wave model in beamforming method (when source is assumed to be in farfield)

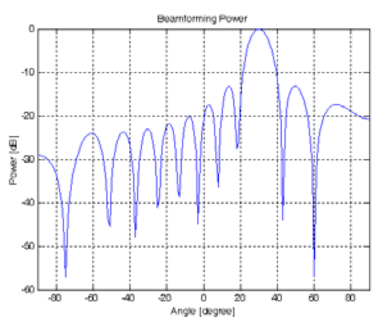

Fig. 3 Simulation result: beamforming power ($\theta_0 = 30^0$, $N = 16$, $d = 5cm$, $f = 10kHz$)

B. *Spherical Wave Model*

When source is located near a hydrophone array, the plane wave model does not satisfy and spherical wave model must be considered (Fig. 4). The pressure for a spherical wave is

$$p_n = \frac{A}{r_{0n}} e^{-jkr_{0n}} \tag{3a}$$

$$r_{0n} = \sqrt{\{(n-1)d - x_0\}^2 + {y_0}^2} . \tag{3b}$$

The beamforming power is the same as Eq. (2a) except the weighting vector as described below.

$$w_n(x, y) = \frac{1}{\sqrt{N}} e^{-jkr_n} \tag{4a}$$

$$r_n = \sqrt{\{(n-1)d - x\}^2 + y^2} \tag{4b}$$

Fig. 5 shows an example of the spherical beamforming method. Although resolution is very poor, the maximum point coincides with the source location.

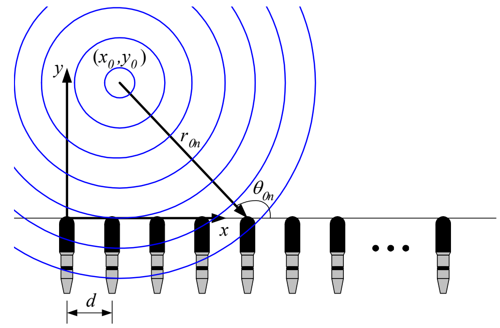

Fig. 4 Spherical wave model in beamforming method (when source is assumed to be in nearfield)

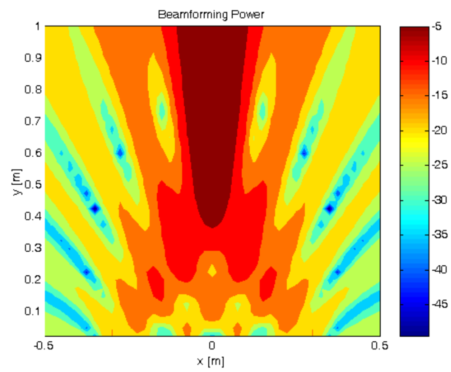

Fig. 5 Simulation result: beamforming power ($(x_0, y_0) = (0, 0.75m)$, $N = 16$, $d = 5cm$, $f = 10kHz$)

III. EFFECTS OF PAHSE DETECTION ERROR

A. *Plane Wave Model*

<u>Array of Two Hydrophones</u>

Let $\Delta\phi_1$ and $\Delta\phi_2$ be the phase detection errors of the first and the second hydrophones. Then the measured acoustic pressures can be expressed as

$$p_1 = Ae^{j\Delta\phi_1} \tag{5a}$$

$$p_2 = Ae^{jkd\sin\theta_0 + j\Delta\phi_2} . \tag{5b}$$

Beamforming power is derived as

$$\Pi(\theta) = 2|A|^2 \cos^2\left[kd(\sin\theta - \sin\theta_0) - \Delta\phi_1 + \Delta\phi_2\right] \tag{6}$$

which is a function of the difference of the phase detection errors $\Delta\phi_1 - \Delta\phi_2$. The estimated incident angle is

$$\hat{\theta} = \sin^{-1}\left[\sin\theta_0 + (\Delta\phi_1 - \Delta\phi_2)/kd\right] \tag{7}$$

which is a nonlinear function of all independent variables. Based on the assumption of small phase detection errors Eq. (7) can be expressed as

$$\hat{\theta} = \theta_0 + \frac{1}{kd\cos\theta_0}(\Delta\phi_1 - \Delta\phi_2) + O\left((\Delta\phi)^2\right) \cdot \tag{8}$$

The error of the estimated angle is proportional to the wavelength and inversely proportional to the distance d. The error has minimum value when $\theta_0 = 0$ or normal incident array. The same phase errors of the both hydrophones lead to no estimation error. Fig. 6(a) compares the cases $\Delta\phi_1 = 0$ and $\Delta\phi_1 > 0$. The estimated incident angle increases when $\Delta\phi_1$ has positive value.

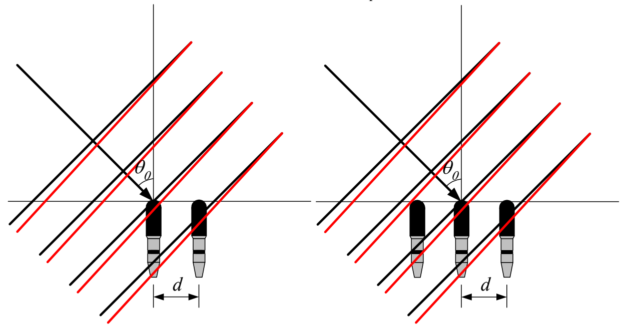

Fig. 6 Incident plane waves when $N = 2$ and $N = 3$. Red lines (brighter lines in BW print) represent phase lead at the first hydrophone.

Array of Three Hydrophones

Measured acoustic pressures are

$$p_1 = Ae^{j\Delta\phi_1} \tag{9a}$$

$$p_2 = Ae^{jkd\sin\theta_0 + j\Delta\phi_2} \tag{9b}$$

$$p_3 = Ae^{2jkd\sin\theta_0 + j\Delta\phi_3} \tag{9c}$$

Beamforming power and estimated incident angle are

$$\Pi(\theta) = \frac{|A|^2}{3}\begin{bmatrix} 3 + 2\cos\{kd(\sin\theta - \sin\theta_0) - \Delta\phi_1 + \Delta\phi_2\} \\ +2\cos\{kd(\sin\theta - \sin\theta_0) - \Delta\phi_2 + \Delta\phi_3\} \\ +2\cos\{2kd(\sin\theta - \sin\theta_0) - \Delta\phi_1 + \Delta\phi_3\} \end{bmatrix} \tag{10}$$

$$\hat{\theta} = \theta_0 + \frac{1}{2kd\cos\theta_0}(\Delta\phi_1 - \Delta\phi_3) + O\left((\Delta\phi)^2\right) \tag{11}$$

As you see in Eq. (11) $\hat{\theta}$ is a function of $\Delta\phi_1 - \Delta\phi_3$ but not $\Delta\phi_2$. The phase error in the second hydrophone has no effect on the result. The effect of the first hydrophone is a half of the two-hydrophone case.

Array of N Hydrophones

Acoustic pressure with phase error $\Delta\phi_n$ at n-th hydrophone is

$$p_n = Ae^{-jk(n-1)d\sin\theta_0}. \tag{12}$$

Beamforming power is then

$$\Pi(\theta) = \frac{|A|^2}{N}\sum_{m,n}\cos[(m-n)kd(\sin\theta - \sin\theta_0) + \Delta\phi_m - \Delta\phi_n] \tag{13}$$

Eq. (13) has the form of

$$\Pi(\theta) = \sum_{m,n} f(\Delta\phi_m - \Delta\phi_n)\cdot \tag{14}$$

The estimated incident angle is rather complex, i.e.

$$\theta_{\max} = \theta_0 + \sum_n a_n\Delta\phi_n + O\left((\Delta\phi)^2\right) \tag{15}$$

where

$$a_n = -\frac{Num}{Den}\frac{1}{kd\cos\theta_0} \tag{16a}$$

$$Num = \frac{N}{2}(N - 2n + 1) \tag{16b}$$

$$Den = \frac{N^2}{12}(N+1)(N-1) \tag{16c}$$

The coefficient a_n represents the amount of contributions to the estimation error. It is proportional to wavelength and inversely proportional to the hydrophone space d as described in the two and three hydrophone cases. The error is minimized when the incident angle is zero. As the number of hydrophone increases the numerator and denominator increases as fast as N^2 and N^4 respectivley. Thus a_n decreases with a factor of $1/N^2$. This means that we have to use as many sensors as possible to reduce the estimation error, which is very simple result. Please see Fig. 7(a) shows the maximum value of $Num/Den = a_n kd\cos\theta_0$ versus N. Fig. 3(b) represents Num/Den versus n when $2 \le N \le 10$. It varies linearly as n changes. It has maximum absolute values at the end of array and has minimum at the center. Therefore, more precise data acquisition is needed near the both ends of array.

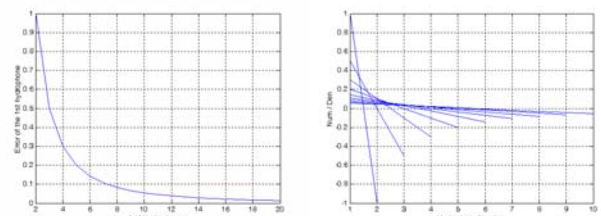

(a) Num/Den versus N (b) Num/Den versus n

Fig. 7 Plots of Num/Den in the coefficient versus N and n

B. Spherical Wave Model

Array of Two Hydrophones

Although at least three hydrophones are needed for source localization, analysis with an array of two hydrophones is tried for better understanding of the results with an array of three or more hydrophones. For spherical wave the measured acoustic pressures with phase errors of $\Delta\phi_1$ and $\Delta\phi_2$ at each hydrophone are

$$p_1 = \frac{A}{r_{01}}e^{-jkr_{01} + j\Delta\phi_1} \tag{17a}$$

$$p_2 = \frac{A}{r_{02}}e^{-jkr_{02} + j\Delta\phi_2}. \tag{17b}$$

The beamforming power is rather complex than that of plane wave model.

$$\Pi(x,y) = \frac{|A|^2}{2}\left[\frac{1}{r_{01}^2} + \frac{1}{r_{02}^2} + \frac{2}{r_{01}r_{02}}\cos\{k(r_{01} - r_{02} - r_1 + r_2) - \Delta\phi_1 + \Delta\phi_2\}\right] \tag{18}$$

It is also a function of the difference of the phase detection errors $\Delta\phi_1 - \Delta\phi_2$ similar to that of a plane wave model. The estimated x and y positions are

$$\hat{x} = x_0 + a_x(\Delta\phi_1 - \Delta\phi_2) + O\left((\Delta\phi)^2\right) \quad (19a)$$

$$\hat{y} = y_0 + a_y(\Delta\phi_1 - \Delta\phi_2) + O\left((\Delta\phi)^2\right) \quad (19b)$$

$$a_x = \frac{1}{k(-\cos\theta_{01} + \cos\theta_{02})} \quad (19c)$$

$$a_y = \frac{1}{k(-\sin\theta_{01} + \sin\theta_{02})}. \quad (19d)$$

Assuming again that the phase errors are small, we can conclude that higher wave number or longer wavelength produces smaller estimation position error. Fig. 8 shows the distribution of $a_x k$, $a_y k$ and $a_r k = \sqrt{(a_x k)^2 + (a_y k)^2}$. Large errors occur when $x = d/2$ and $y = 0$. Smaller errors are obtained when $y/x \approx \tan 50^o$ and the source is nearer to the array.

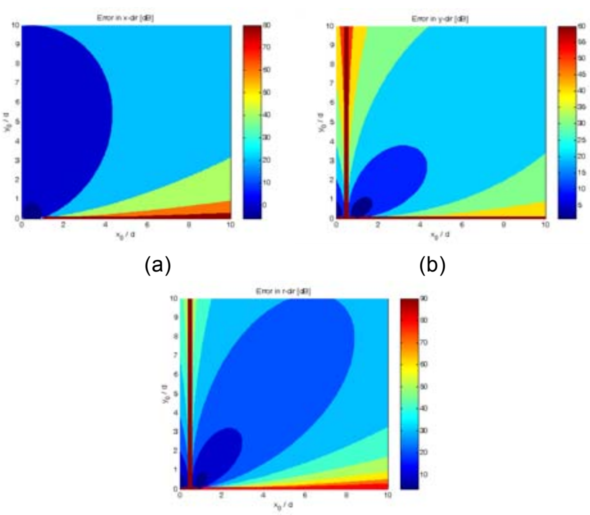

(a) (b)

(c)

Fig. 8 Effect of phase error by the first hydrophone on the estimated positions (a) $a_x k$ (b) $a_y k$ and (c) $a_r k$

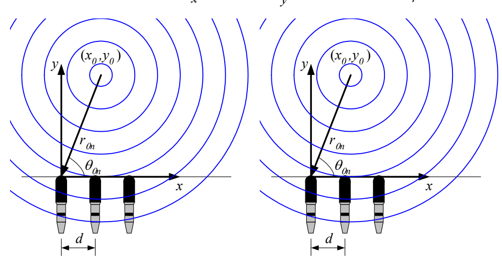

Fig. 9 Incident spherical waves when $N = 2$ and $N = 3$.

<u>Array of Three Hydrophones</u>

When there are three hydrophones, their measured acoustic pressures are described as

$$p_1 = \frac{A}{r_{01}} e^{-jkr_{01} + j\Delta\phi_1} \quad (20a)$$

$$p_2 = \frac{A}{r_{02}} e^{-jkr_{02} + j\Delta\phi_2} \quad (20b)$$

$$p_3 = \frac{A}{r_{03}} e^{-jkr_{03} + j\Delta\phi_3}, \quad (20c)$$

Then the beamforming power is

$$\Pi(x,y) = \frac{|A|^2}{3}\left[\begin{array}{l} \frac{1}{r_{01}^2} + \frac{1}{r_{02}^2} + \frac{1}{r_{03}^2} \\ + \frac{2\cos[k(r_{01} - r_{02} - r_1 + r_2) - \Delta\phi_1 + \Delta\phi_2]}{r_{01} r_{02}} \\ + \frac{2\cos[k(r_{02} - r_{03} - r_2 + r_3) - \Delta\phi_2 + \Delta\phi_3]}{r_{02} r_{03}} \\ + \frac{2\cos[k(r_{01} - r_{03} - r_1 + r_3) - \Delta\phi_1 + \Delta\phi_3]}{r_{01} r_{03}} \end{array}\right]. \quad (21)$$

The estimated x and y coordinates are

$$\hat{x} = x_0 + \sum_n a_{xn}\Delta\phi_n + O\left((\Delta\phi)^2\right) \quad (22a)$$

$$\hat{y} = y_0 + \sum_n a_{yn}\Delta\phi_n + O\left((\Delta\phi)^2\right), \quad (22b)$$

where

$$a_{xn} = \frac{Num_{xn}}{Den_x}, \quad a_{yn} = \frac{Num_{yn}}{Den_y} \quad (23a)$$

and

$$Num_{x1} = \frac{1}{r_{01} r_{02}}\left(-\frac{x_0}{r_{01}} + \frac{x_0 - d}{r_{02}}\right) + \frac{1}{r_{01} r_{03}}\left(-\frac{x_0}{r_{01}} + \frac{x_0 - 2d}{r_{03}}\right) \quad (23b)$$

$$Num_{x2} = \frac{1}{r_{01} r_{02}}\left(\frac{x_0}{r_{01}} + \frac{x_0 - d}{r_{02}}\right) + \frac{1}{r_{02} r_{03}}\left(-\frac{x_0 - d}{r_{02}} + \frac{x_0 - 2d}{r_{03}}\right) \quad (23c)$$

$$Num_{x3} = \frac{1}{r_{01} r_{03}}\left(\frac{x_0}{r_{01}} - \frac{x_0 - 2d}{r_{03}}\right) + \frac{1}{r_{02} r_{03}}\left(\frac{x_0 - d}{r_{02}} - \frac{x_0 - 2d}{r_{03}}\right) \quad (23d)$$

$$Den_x = \frac{k}{r_{01} r_{02}}\left(\frac{x_0}{r_{01}} - \frac{x_0 - d}{r_{02}}\right)^2 + \frac{k}{r_{01} r_{03}}\left(\frac{x_0}{r_{01}} - \frac{x_0 - 2d}{r_{03}}\right)^2 + \frac{k}{r_{02} r_{03}}\left(\frac{x_0 - d}{r_{02}} - \frac{x_0 - 2d}{r_{03}}\right)^2 \quad (23e)$$

$$Num_{y1} = \frac{1}{r_{01} r_{02}}\left(-\frac{y_0}{r_{01}} + \frac{y_0}{r_{02}}\right) + \frac{1}{r_{01} r_{03}}\left(-\frac{y_0}{r_{01}} + \frac{y_0}{r_{03}}\right) \quad (23f)$$

$$Num_{y2} = \frac{1}{r_{01} r_{02}}\left(\frac{y_0}{r_{01}} + \frac{y_0}{r_{02}}\right) + \frac{1}{r_{02} r_{03}}\left(-\frac{y_0}{r_{02}} + \frac{y_0}{r_{03}}\right) \quad (23g)$$

$$Num_{y3} = \frac{1}{r_{01} r_{03}}\left(\frac{y_0}{r_{01}} - \frac{y_0}{r_{03}}\right) + \frac{1}{r_{02} r_{03}}\left(\frac{y_0}{r_{02}} - \frac{y_0}{r_{03}}\right) \quad (23h)$$

$$Den_y = \frac{k}{r_{01} r_{02}}\left(\frac{y_0}{r_{01}} - \frac{y_0}{r_{02}}\right)^2 + \frac{k}{r_{01} r_{03}}\left(\frac{y_0}{r_{01}} - \frac{y_0}{r_{03}}\right)^2 + \frac{k}{r_{02} r_{03}}\left(\frac{y_0}{r_{02}} - \frac{y_0}{r_{03}}\right)^2 \quad (23i)$$

Figs. 10 and 11 shows the effect of phase errors by the first and second hydrophones on the estimated position. Unlike the case of two hydrophones, large error along $x = const.$ does not appear. Error in x-coord is small in the front direction whereas Error in y-coord is in the direction of $\theta \approx 45^o$. Large error at $y = 0$ still happens.

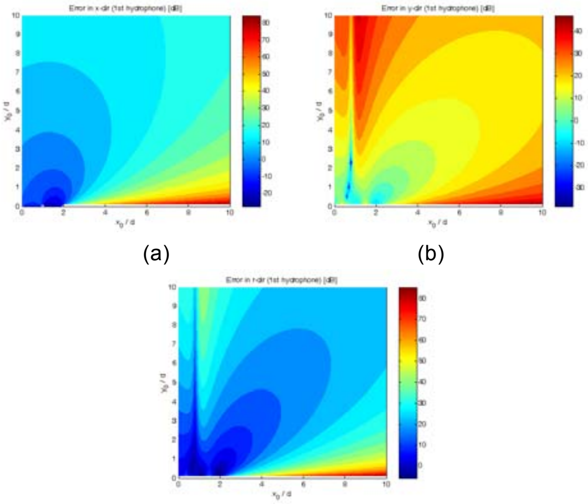

(a) (b)

(c)

Fig. 10 Effect of phase error by the first hydrophone on the results (a) $a_x k$ (b) $a_y k$ and (c) $a_r k$

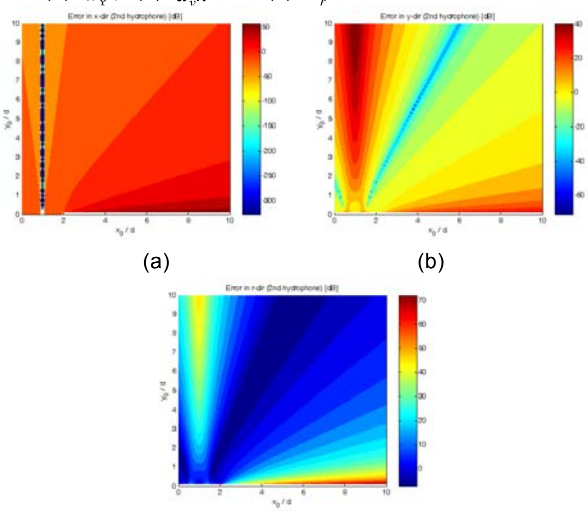

(a) (b)

(c)

Fig. 11 Effect of phase error by the second hydrophone on the result (a) $a_x k$ (b) $a_y k$ and (c) $a_r k$

<u>Array of N Hydrophones</u>

Acoustic pressure with phase error $\Delta\phi_n$ at n-th hydrophone is

$$p_n = \frac{A}{r_{0n}} e^{-jkr_{0n} + j\Delta\phi_n}. \tag{24}$$

The estimated positions are

$$\hat{x} = x_0 + \sum_n a_{xn} \Delta\phi_n + O\left((\Delta\phi)^2\right) \tag{25a}$$

$$\hat{y} = y_0 + \sum_n a_{yn} \Delta\phi_n + O\left((\Delta\phi)^2\right) \tag{25b}$$

where

$$a_{xn} = \frac{Num_{xn}}{Den_x}, \quad a_{yn} = \frac{Num_{yn}}{Den_y} \tag{25c,d}$$

$$Num_{xn} = \sum_{\substack{m \\ m \neq n}} \frac{1}{r_{0n} r_{0m}} \left(\frac{x_0 - (m-1)d}{r_{0m}} - \frac{x_0 - (n-1)d}{r_{0n}} \right) \tag{25e}$$

$$Den_x = \sum_{\substack{m,n \\ m > n}} \frac{k}{r_{0n} r_{0m}} \left(\frac{x_0 - (m-1)d}{r_{0m}} - \frac{x_0 - (n-1)d}{r_{0n}} \right)^2 \tag{25f}$$

$$Num_{yn} = \sum_{\substack{m \\ m \neq n}} \frac{1}{r_{0n} r_{0m}} \left(\frac{y_0}{r_{0m}} - \frac{y_0}{r_{0n}} \right) \tag{25g}$$

$$Den_y = \sum_{\substack{m,n \\ m > n}} \frac{k}{r_{0n} r_{0m}} \left(\frac{y_0}{r_{0m}} - \frac{y_0}{r_{0n}} \right)^2 \tag{25h}$$

The coefficient a_{nx} and a_{ny} represent the amounts of contributions to the estimated position errors in x and y coordinates. It is proportional to wavelength as in the plane wave case. Fig. 12(a) plots a_{nx} and a_{ny} versus hydrophone position when $N = 8$. As shown in the upper plot, a_{nx} is an odd function of n. It has maximum absolute values at the both ends and zero value at the center. This property is the same as the plane wave case. a_{ny} (shown in the lower plot) is an even function of n. It has local maximum at the center and minimum values at the ends. Tow zero values are obtained somewhere between the maximum and minimum points. Fig. 12(b) shows a_{nx} and a_{ny} when $N = 16$. Similar patterns are obtained. Maximum absolute values are much smaller than in the case of $N = 8$. Fig. 12(c) shows the maximum

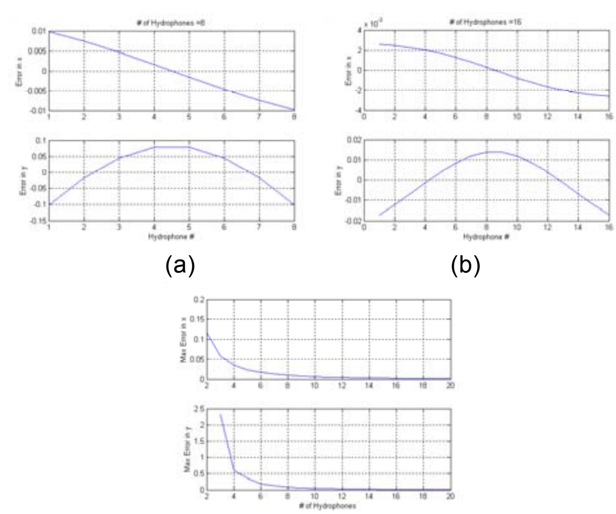

(a) (b)

(c)

Fig. 12 Plots of the coefficients a_{nx} and a_{ny} (a) a_{nx} and a_{ny} versus n ($N = 8$) (b) a_{nx} and a_{ny} versus n ($N = 16$) (c) Maximum absolute values of a_{nx} and a_{ny} versus N

absolute values versus N. It decreases rapidly as N increases. Thus we can conclude that as many number of hydrophones are needed as possible to minimize estimation errors.

III. SOUND FIELDS WITH FREE SURFACE RELFECTIONS

As shown in Fig. 13 source localization with one vertical line array is considered. The number of hydrophones is 16 and they are evenly distributed. Their directivities are assumed to be omni-directional. A projector, a sound source located at a certain depth, radiates spherical waves. When there is no reflection, no estimation error is obtained for the conventional beamforming algorithms. When surface reflection exists the estimated location does not agree to the true position. Fig. 14 shows the estimated source location for free surface reflection condition. Because the aperture size is zero along the x-axis large error is obtained. It will be improved by adding horizontal hydrophone array. Restricted to the z-axis, the estimated position oscillates according to the change of frequency. At the first local maximum (1.2kHz) pressure phase difference from no reflection has a positive slope, whereas at the first local minimum (1.8kHz) it has a negative slope. At the frequency of 5.0kHz the aperture size covers over more than two periods of fluctuations. Over that frequency (5.0kHz) the reflection effect is negligible for the source localization.

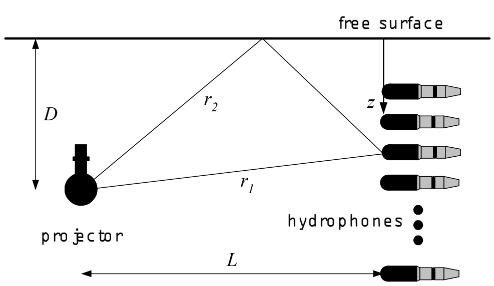

Fig. 13 Configuration of beamforming analysis under the free surface reflections

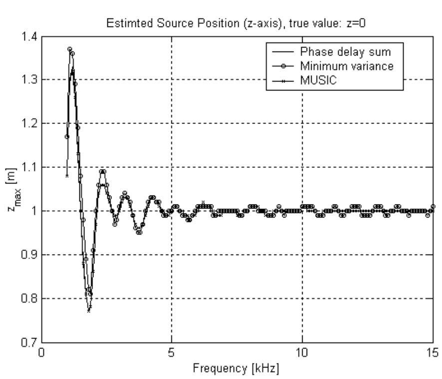

Fig. 14 Estimated source position for free surface reflection condition (first local maximum: 1.2kHz, first local minimum: 1.8kHz, scanning window size: 1m(x)x1m(z), step: 0.01m)

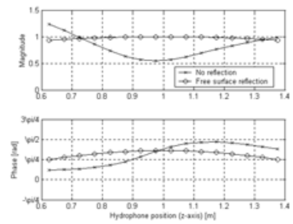

(a) frequency=1.2kHz

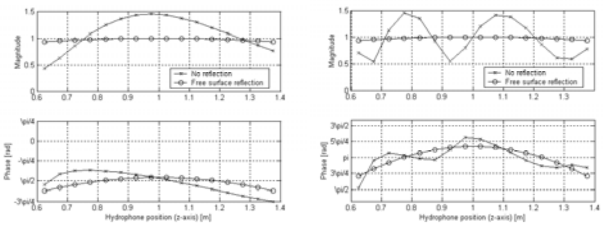

(b) frequency=1.8kHz (c) frequency=5.0kHz

Fig. 15 Magnitude and phase at the hydrophone position for free surface reflection condition

IV. CONCLUSIONS

The effect of phase distortion by surface reflection on source localization is described. A monopole source at shallow water depth and nearfield measurements are assumed. The free surface reflection is assumed to be governed by the pressure release condition. The conventional beamforming algorithm is applied for localizing the source. For better understanding, conditions of no reflection is also considered. Although wave reflections lead phase change at the hydrophone positions, the effect is negligible if one use a hydrophone array whose aperture size is longer than 2.5λ. Therefore, we can conclude that the reflection by the free surface in an anechoic tank need not to be considered if the array aperture is larger than 2.5 times of the wavelength.

Acknowledgements

This work is the part of the results of “Enhancement of Design Engineering Technology for Ocean Development” supported by Korea Research Council of Public Science and Technology (KORP) and “Development of Acoustic-based Underwater Image Communication System” supported by Ministry of Commerce, Industry and Energy (MOCIE), Korea.

References

[1] Y.-K. Lim et al., “Development of test techniques for an underwater acoustic basin,” KRISO/KORDI Project Report, 2001.

[2] S. U. Pillai, *Array Signal Processing*, New York: Springer-Verlag, 1989.

[3] A. B. Baggeroer, W. A. Kuperman, and P. N. Mikhalevsky, “An overview of matched field methods in ocean acoustics,” *IEEE Journal of Oceanic Engineering*, Vol. 18, No. 4, pp. 401-424, October 1993.

[4] Y.-C. Choi and Y.-H. Kim, “Source identification in an interior sound field,” *Journal of Korean Society for Noise and Vibration Engineering*, Vol. 12, No. 7, pp. 520-526, 2002.